https://dx.doi.org/10.1016/j.envpol.2021.118266

Estimating emissions of cooking organic aerosols in winter over the Pearl River Delta region, China

Li Xing[1], Tzung-May Fu[2,3], Tengyu Liu[4,8], Yiming Qin[5], Chak K. Chan[4], Hai Guo[6], Dawen Yao[6], Jianwu Yan[1], Xin Long[2,3], Keqin Duan[1], Guohui Li[7]

1 School of Geography and Tourism, Shaanxi Normal University, Xi'an, Shaanxi, China

2 State Environmental Protection Key Laboratory of Integrated Surface Water-Groundwater Pollution Control, School of Environmental Science and Engineering, Southern University of Science and Technology, Shenzhen, Guangdong, China

3 Shenzhen Institute of Sustainable Development, Southern University of Science and Technology, Shenzhen, Guangdong, China

4 School of Energy and Environment, City University of Hong Kong, Hong Kong, China

5 School of Engineering and Applied Sciences, Harvard University, Cambridge, Massachusetts, United States

6 Department of Civil and Environmental Engineering, The Hong Kong Polytechnic University, Hong Kong, China

7 Key Laboratory of Aerosol Chemistry and Physics, SKLLQG, Institute of Earth Environment, Chinese Academy of Sciences, Xi'an, Shaanxi, China

8 now at: School of Atmospheric Sciences, Nanjing University, Nanjing, Jiangsu, China

Corresponding author: Li Xing (xingli@snnu.edu.cn)

Abstract: Cooking is an important source of organic aerosols (OA), particularly in urban areas, but it has not been explicitly included in current emission inventories in China. This study estimated cooking emissions during winter over the Pearl River Delta (PRD) region, one of the largest economic and most populous regions in China. Using the hourly measured cooking organic aerosol (COA) concentrations at two sites in Hong Kong and Guangzhou, population density, and daily per capita COA emissions, we determined the spatial and temporal distribution of COA emissions over the PRD region. By using the estimated COA emissions and the Weather Research and Forecasting model coupled with chemistry (WRF-Chem) model, we reproduced the diurnal cycles of COA concentrations at the PolyU site in Hong Kong and Panyu site in Guangzhou. We also resolved the different patterns between weekdays and weekends, corresponding to daily per capita COA emissions of 209 mg day^{-1} $person^{-1}$ on weekends and 149 mg day^{-1} $person^{-1}$ on weekdays. The averaged COA concentration during wintertime over the urban areas of the PRD region was 0.7 μg m^{-3} on the daily average, contributing 5.1% to the OA concentrations. The contribution of COA to OA during mealtime was 6.6%, which was higher than that of the daily average. The total COA emissions in winter over the PRD region were estimated to be 3.5×10^{8} g $month^{-1}$, adding 34.8% to the total primary organic aerosol emissions. Our study therefore highlights the importance of cooking activities to OA concentrations in winter over the PRD region.

1. Introduction

Organic aerosols (OA) are important components of $PM_{2.5}$, constituting a large fraction of the mass of $PM_{2.5}$ worldwide.[1,2] OA are often composed of numerous organic compounds in the atmosphere. Due to their complexity, OA are usually categorized into two types, namely primary OA (POA) with direct emissions from various combustion sources such as fossil fuel combustion and biomass burning, and secondary OA (SOA) formed from the oxidation of volatile organic compounds (VOCs), aqueous-phase reactions of carbonyls, and oxidation of some gaseous species evaporated from POA in the atmosphere.[3,4]

In China, chemical transport models for OA simulations have been improved significantly in recent years, but most model results continue to underestimate the observed OA concentrations.[5-13] The underestimation has been shown to originate from under-predicted SOA formation, or misrepresented or missing sources of POA in the emission inventories. One missing primary source of POA in emission inventories is cooking OA (COA).[14]

Using aerosol mass spectrometer (AMS) measurements with positive matrix factorization (PMF) analyses, several studies have reported that COA is an important component of OA worldwide.[15-30] In Europe, the reported contributions of COA to OA ranged from 17% to 30%.[15,17,18,20] Sun et al.[24] reported that COA contributed 16% to the total OA mass in New York City, US and Xu et al.[19] estimated the COA contribution to be 12%–20% in Georgia, US. In China, the mass fractions of COA in OA in Beijing were shown to be 10%–15% across different seasons.[25] The contributions of COA to OA in winter were found to be relatively higher during non-haze days (11.5% in Beijing and 9.3% in Xi'an), compared with those during haze days (5.8% in Beijing and 3.6% in Xi'an).[21] In the Pearl River Delta (PRD) region in southern China, the mass fractions of COA in OA were higher in urban areas (20.6% - 34.6%) than those in the rural areas (6.5% - 9.6%).[23,28-30]

Cooking emissions are affected by various factors, such as cooking style, oils, food ingredients, temperature, duration, and ventilation.[31] Chinese-style cooking is popular worldwide because of its versatile food ingredients, special seasoning, and cooking style, and results in different emissions compared with western-style cooking.[32] Using the observed COA concentrations, Fountoukis et al.[33] estimated the COA emissions in Paris to be ~80 mg day^{-1} $person^{-1}$. They incorporated COA emissions into a three-dimensional regional chemical transport model (PMCAMx) based on population density and found that the model could reproduce the observed diurnal profiles of COA concentrations at two sites in

Paris. Ots et al.[22] estimated COA emissions to be 320 mg day^{-1} $person^{-1}$ in the UK and the annual COA emissions to be 7.4 Gg $year^{-1}$, adding 10% to the officially reported national anthropogenic $PM_{2.5}$ emissions (82 Gg $year^{-1}$ in 2012).

The PRD region is one of the largest economic regions in China that is highly populated. Although $PM_{2.5}$ concentrations in the PRD region have declined in recent years due to emission control strategies,[34] COA emissions could potentially be important emission sources due to the high population density in the PRD region[35]. Ye et al.[35] showed that Guangzhou, in the PRD region, was one of the four most populous cities in mainland China. The population density in Hong Kong was also very high with about 6777 people km^{-2} on average.[36] In this study, we used the AMS-measured COA concentrations in Hong Kong and Guangzhou and the population density data from the LandScan database to construct gridded COA emissions in the PRD region.[27,37] We added a COA tracer in the Weather Research and Forecasting Model coupled with Chemistry (WRF-Chem) model, and simulated COA concentrations in the PRD region with the constructed COA emissions. The simulated COA concentrations were compared with observations in Hong Kong and Guangzhou by adjusting the emissions multiple times, until the model could capture the diurnal cycles of observed COA concentrations. The model results were then validated with observed COA concentrations at two other sites in Shenzhen and Guangzhou. Finally, the total winter COA emissions in the PRD region were estimated.

2. Methods

2.1 Model description

In this study, we used the WRF-Chem model developed by Li et al.[38-41] The model included the gas-phase chemical mechanism "Statewide Air Pollution Research Center-99" (SAPRC-99), and the aerosol module from the "Community Multi-scale Air Quality Model" (CMAQ)/Model 3.[42] A volatility basis set (VBS) approach with aging was used to simulate OA.[40] The POA components of traffic and biomass burning were represented by nine surrogate species with saturation concentrations (C^*) from 10^{-2} to 10^6 μg m^{-3} at 298 K, respectively,[43] and were assumed to be semi-volatile and photochemically reactive.[3] SOA formation from each anthropogenic or biogenic precursor was simulated using four semi-volatile VOCs with saturation concentrations of 1, 10, 100, and 1000 μg m^{-3} at 298 K. COA concentrations could not be predicted using the WRF-Chem model because this model did not include the chemical species of COA. Moreover, COA emissions were not included in the current widely-used Multi-resolution Emission Inventory for China (MEIC).[14]

Here, a COA tracer was incorporated into the WRF-Chem model. Although COA can undergo further photochemical reactions in the atmosphere[44], the COA tracer was assumed to be non-volatile and did not evolve chemically and was incorporated into the total OA mass for the calculation of absorptive partitioning of SOA. Several studies have reported that cooking also contributes to SOA formation, but significant uncertainties remain regarding the aging rates and yields of SOA from the VOCs emitted from different cooking styles and oils.[45-47] More SOA yields measurements from semi-volatile and intermediate volatile organic gases are needed before this process can be incorporated into chemical models.[22]

The WRF-Chem model domain was configured with 400 × 400 grid cells centered at 23 °N and 115 °E (Figure 1). The horizontal resolution was 6 km and the model consisted of 35 vertical layers. The simulation chose the microphysical parameterization scheme by Morrison et al.[48], Goddard shortwave and longwave radiation schemes,[49,50] Mellor-Yamada-Janjić (MYJ) surface layer scheme,[51] MYJ turbulent kinetic energy planetary boundary layer scheme,[47] and Unified Noah land-surface model.[52] The National Centers for Environmental Prediction (NCEP) 1º × 1º reanalysis data (https://rda.ucar.edu/datasets/ds083.2/) was used for the meteorological initial and boundary conditions. The chemical initial and boundary conditions were provided by the Model for OZone And Related chemical Tracers (MOZART) output at 6 h intervals.[53] To estimate COA emissions in winter over the PRD region, we simulated the OA and $PM_{2.5}$ concentrations from December 27, 2017 to January 15, 2018. The spin-up time was 2 d.

The anthropogenic emission inventory of MEIC was used in the simulation. It included the agricultural, industrial, power plant, residential, and transportation sectors, with the base year of 2016.[14,54] The biomass burning emissions used the FINN fire inventory from the National Center for Atmospheric Research in US.[55,56] The biogenic emissions were calculated online from the Model of Emissions of Gases and Aerosols from Nature (MEGAN) module.[57]

2.2 Observation data

OA was measured at an urban roadside site at the Hong Kong Polytechnic University (PolyU) (22.30 °N and 114.18 °E) from December 27, 2017 to January 15, 2018 and Panyu Atmospheric Composition station in Guangzhou (Panyu) (23.00 °N, 113.21 °E) from November 7, 2014 to January 3, 2015 using a high-resolution time-of-flight aerosol mass spectrometer (HR-ToF-AMS, Aerodyne Research Incorporated, Billerica, MA). Details of the measurements are provided in Liu et al.[27] and Qin et al.[30] Five factors for the measured OA at the PolyU site were identified using the PMF analysis, including two primary

emission-dominated factors (hydrocarbon-like OA (HOA) and COA), and three oxygenated factors (OOA1, OOA2, and OOA3) associated with different oxidation levels. The OA factors at the Panyu site included three primary-dominated factors (HOA, COA, biomass-burning-related OA (BBOA)), and two oxygenated factors (SVOOA and LVOOA). The PolyU site was located less than 1 km from the Tsim Sha Tsui commercial areas with a large number of restaurants (Figure S1). The Panyu site was surrounded by residential neighborhoods.[30] The contributions of COA to OA for both sites were significant due to the intensive emissions, and we used the analyzed COA concentrations for the PolyU and Panyu sites to validate model results and estimate COA emissions.

To evaluate the model performance, the measured hourly $PM_{2.5}$ concentrations over the model domain were downloaded from the website of China's Ministry of Ecological Environment (http://www.aqistudy.cn/). The monitoring sites are shown in Figure 1.

2.3 Estimation of COA emissions

The COA emissions over the model domain were estimated using population density and observed diurnal profiles of COA concentrations at the PolyU and Panyu sites.[22] Figure 1 shows the population density for 2017 from the LandScan dataset. We estimated the spatiotemporal distribution of COA emissions based on the population density, observed diurnal profiles of COA concentrations at the PolyU and Panyu sites on the assumption that the daily per capita cooking emission value was 320 mg day^{-1} $person^{-1}$.[22] We then compared the simulated COA concentrations with the observations at the PolyU and Panyu sites, and adjusted the daily per capita cooking emission value until the model could reproduce the magnitude and variations of observed COA concentrations at the PolyU and Panyu sites.

2.4 Statistical indexes for model evaluation

The following numerical metrics were employed for model evaluation: the normalized mean bias (*NMB*) and index of agreement (*IOA*).

$$NMB = \frac{\frac{1}{N}\sum_{i=1}^{N}(P_i - O_i)}{\bar{O}} \times 100\% \quad (1)$$

$$IOA = 1 - \frac{\sum_{i=1}^{N}(P_i - O_i)^2}{\sum_{i=1}^{N}(|P_i - \bar{O}| + |O_i - \bar{O}|)^2} \quad (2)$$

where P_i and O_i are the model-predicted and observed concentrations of the chemical species i, respectively, N is the number of model and observation data used for comparisons, and $\bar{O}$ is the average concentration of observations. An *IOA* of 1 indicates a perfect agreement between the model and the

observation. A zero or negative *IOA* indicates that the model could not explain any of the observational variations.

3. Results and Discussion

Figure 2a indicates the temporal profiles of the simulated and observed $PM_{2.5}$ concentrations averaged over all monitoring sites in the model domain. The model generally captured the temporal change of $PM_{2.5}$ concentrations, but predicted more distinct variations than those of the observations. The *NMB* and *IOA* were 9.38% and 0.72, respectively.

Figure 2(b-d) presents the temporal variations of the simulated and observed HOA and SOA concentrations at the PolyU site from December 27, 2017 to January 15, 2018. The model reproduced the diurnal variations of HOA at the PolyU site, particularly from January 4 to 15, 2018 (Figure 2b). HOA was mainly associated with traffic emissions and showed a distinct peak during the morning rush hours, while the HOA concentrations during the evening rush hours were not as high as that of the morning rush hours. The *NMB* and *IOA* for HOA were -5.62% and 0.70, respectively. The model reproduced the observed variations of COA, with *NMB* and *IOA* to be 0.83% and 0.49, respectively (Figure 2c). The COA concentrations generally showed two peaks during the lunchtime and dinnertime. The model simulated the relatively high observed SOA concentrations during the first half of the simulation periods, and the relatively low SOA concentrations during the later periods (Figure 2c). The SOA simulation results were inferior to those of HOA and COA, with *NMB* and *IOA* to be -13.05% and 0.48, respectively.

We further explored the diurnal variations of COA at the PolyU and Panyu sites on weekdays and weekends. The observed COA concentrations on the weekdays had two distinct peaks during lunchtime (12:00–14:00 local time) and dinnertime (19:00–21:00 local time) for both the PolyU and Panyu sites, with maximum concentrations of 2.0 and 1.3 μg m^{-3} during lunchtime and 2.5 and 3.0 μg m^{-3} during dinnertime, respectively (Figure 3a and Figure 3c). The relatively high ratio of COA concentrations during lunchtime over that during dinnertime at the PolyU site indicated that the PolyU site was close to commercial areas with large COA emissions during lunchtime and dinnertime, while the relatively low ratio at the Panyu site reflected that the Panyu site was surrounded by the residential areas with low COA emissions during lunchtime. The observed weekend COA concentrations presented one peak during dinnertime, with a maximum concentration of 3.2 and 4.4 μg m^{-3} (Figure 3b and Figure 3d), which were significantly higher than that on weekdays, while the COA concentrations during lunchtime on weekends did not show an obvious increase. The high COA concentrations during dinnertime on weekends at the

PolyU site were mainly due to the high COA emissions from a large number of restaurants near the Tsim Sha Tsui area, located less than 1 km from the PolyU site (Figure S1). The Panyu site is also surrounded by residential neighborhoods,[30] resulting in high COA concentrations during dinnertime. The daily averaged COA concentration during weekends was 1.4 μg m^{-3} and 1.6 μg m^{-3} for the PolyU and Panyu sites, which were higher than those of 1.1 μg m^{-3} and 1.3 μg m^{-3} on weekdays. The model generally captured diurnal variations on weekdays and weekends for the PolyU and Panyu sites.

To further validate the estimated COA emissions, we compared the simulated COA concentrations with observations at two urban sites in Shenzhen (113.90 °E, 22.60 °N) and Guangzhou (113.21 °E, 23.08 °N) in winter, respectively.[23,58] Compared with Figure 3 in Cao et al.[23], Figure S2 shows that the model reproduced the observed COA peak during lunchtime of approximately 2 μg m^{-3}. Although the model also simulated the COA peak during dinnertime with a maximum concentration of 2.0 μg m^{-3}, it still underestimated the observed COA concentrations of ~ 6 μg m^{-3} during dinnertime and nighttime. One reason was that the observed COA concentrations at the PolyU site during the nighttime was relatively low, and therefore, the estimated COA emissions during nighttime were at a low level based on our methods. The modeled COA contribution to OA in Shenzhen was 8.0%, with an underestimation of the observed fraction of 20.6%. The modeled COA concentrations at the Guangzhou site was 2.0 μg m^{-3} and contributed 16.6% to OA concentrations, which was comparable with the observed OA mass fractions of 18%, but underestimated the observed COA concentrations of 3.1 μg m^{-3}.[58] Figure S3 shows the simulated diurnal cycles of COA at the urban site in Guangzhou, which were in the range of the observed COA diurnal variations during the non-pollution and pollution periods (Figure 5 from Guo et al.[58]). That notwithstanding, the model performance for the COA simulation in Shenzhen and Guangzhou was acceptable to some extent, and the model simulations were useful for estimating COA emissions over the PRD region.

Based on the minimal difference between the simulated and observed COA concentrations at the PolyU site, the best estimation of daily per capita COA emission was 209 mg day^{-1} $person^{-1}$ on weekends and 149 mg day^{-1} $person^{-1}$ on weekdays over the PRD region, which was lower than that in the UK,[22] but higher than that in France.[33] This was probably caused by the differences in cooking styles. The most popular Cantonese cooking style in the PRD region is usually frying, stewing, or braising, while in the UK it is grilling, frying, or even deep-frying, all of which produce higher OA emissions. Figure 4 shows the diurnal variations of COA emission percentages on weekdays and weekends in the PRD region.

Consistent with the observed high COA concentrations, COA emission percentages during dinnertime were the highest on both weekdays and weekends, contributing 31.8% and 28.3% to total daily COA emissions on weekdays and weekends, respectively. The COA emission percentages during lunchtime were 24.4% and 24.5% on weekdays and weekends, respectively. The COA emissions between the lunchtime and dinnertime were much higher on weekends than those on weekdays, reflecting that people have more casual time for eating on weekends. The COA emissions at night were very low and did not exceed 2% for each hour, especially on weekdays.

Figure 5 demonstrates the spatial distribution of the estimated COA emissions and modeled COA concentrations averaged over the simulation period in the PRD region. The high COA emissions (exceeding 30.0×10^3 g km^{-2} month^{-1}) originated in the central area of the PRD region due to the high population density, particularly in the city centers, with emissions higher than 80×10^3 g km^{-2} month^{-1} (Figure 4a). The COA emissions in the marginal areas of the PRD region were significantly lower and generally did not exceed 10.0×10^3 g km^{-2} month^{-1}. The total COA emissions in winter over the PRD region were estimated to be 3.5×10^8 g month^{-1}. The total primary organic carbon emissions in winter over the PRD region from the MEIC emission inventory were 6.1×10^8 g month^{-1}.[54] COA emissions added 34.8% to the total primary OA emissions (multiplied by 1.65)[59], thereby making up an important source of primary OA during wintertime over the PRD region. The simulated COA concentrations were also at a high level in the central area of the PRD region (Figure 4b). COA emissions and concentrations in Guangzhou were the highest over the PRD region, exceeding 160.0×10^3 g km^{-2} month^{-1} and 2.0 μg m^{-3}, respectively. Unlike the relatively high COA emissions in Dongguan, Shenzhen, and Hong Kong, that are located in the southeast of Guangzhou, the simulated COA concentrations in Foshan, Zhongshan, and Zhuhai in the southwest of Guangzhou were higher than those in the southeast of Guangzhou. Using the land-use data in 2018 from the remote sensing images of Landsat 8 to identify the urban areas in the PRD region (http://www.resdc.cn, Figure S4), the COA concentration in winter was 0.7 μg m^{-3} on the daily average and 1.0 μg m^{-3} during the mealtime in the urban areas of the PRD region, contributing 5.1% and 6.6% to the urban OA concentrations, respectively. The COA concentration and contribution to OA in the urban areas were significantly higher than those of 0.35 μg m^{-3} and 3.2% contribution on the daily average over the entire PRD region.

In this study, COA emissions, which have not been included in the existing emission inventories, were estimated during winter over the PRD region. The best estimation of COA emissions in winter over the

PRD region was 3.5×10^8 g $month^{-1}$, adding 34.8% to the total primary OA emissions. The results indicate that COA emissions over the PRD region during winter are important primary OA sources. Ots et al.[22] claimed that the PMF analysis based on AMS measurements may overestimate COA concentrations by a factor of 2. Even making an allowance for this overestimation, the COA emissions still contributed 17.4% to the primary OA emissions over the PRD region during winter. The average COA concentration during winter over the urban areas of PRD region was 0.7 μg m^{-3}, contributing 5.1% to the total OA concentrations.

The estimation of COA emissions in this study was based on treating COA as a non-volatile tracer that is primarily emitted in the model. Given that laboratory studies[44-46] have shown that COA as well as VOCs from cooking also contribute to SOA formation, further studies are needed to parameterize the aging rates and SOA yields of primary COA emissions, so that the model can accurately simulate both POA and SOA concentrations from cooking activities.

Acknowledgements:

This study is supported by the National Natural Science Foundation of China (Grant nos. 41807310), the Natural Science Foundation of Shaanxi Province (2020JQ-414), and the Fundamental Research Funds for the Central Universities (GK202003066).

References:

(1) Zhang, Q.; Jimenez, J. L.; Canagaratna, M. R.; Allan, J. D.; Coe, H.; Ulbrich, I.; Alfarra, M. R.; Takami, A.; Middlebrook, A. M.; Sun, Y. L.; Dzepina, K.; Dunlea, E.; Docherty, K.; De- Carlo, P. F.; Salcedo, D.; Onasch, T.; Jayne, J. T.; Miyoshi, T.; Shimono, A.; Hatakeyama, S.; Takegawa, N.; Kondo, Y.; Schneider, J.; Drewnick, F.; Borrmann, S.; Weimer, S.; Demerjian, K.; Williams, P.; Bower, K.; Bahreini, R.; Cottrell, L.; Griffin, R. J.; Rautiainen, J.; Sun, J. Y.; Zhang, Y. M.; Worsnop, D. R. Ubiquity and dominance of oxygenated species in organic aerosols in anthropogenically-influenced Northern Hemisphere midlatitudes. *Geophys. Res. Lett.* **2007**, 34, L13801.

(2) Jimenez, J. L.; Canagaratna, M. R.; Donahue, N. M.; Prévôt, A. S.; Zhang, Q.; Kroll, J. H.; DeCarlo, P. F.; Allan, J. D.; Coe, H.; Ng, N. L.; Aiken, A. C.; Docherty, K. S.; Ulbrich, I. M.; Grieshop, A. P.; Robinson, A. L.; Duplissy, J.; Smith, J. D.; Wilson, K. R.; Lanz, V. A.; Hueglin, C.; Sun, Y. L.; Tian, J.; Laaksonen, A.; Raatikainen, T.; Rautiainen, J.; Vaattovaara, P.; Ehn, M.; Kulmala, M.; Tomlinson, J. M.; Collins, D. R.; Cubison, M. J.; Dunlea, E. J.; Huffman, J. A.; Onasch, T. B.; Alfarra, M. R.; Williams, P. I.; Bower, K.; Kondo, Y.; Schneider, J.; Drewnick, F.; Borrmann, S.; Weimer, S.; Demerjian, K.; Salcedo, D.; Cottrell, L.; Griffin, R.; Takami, A.; Miyoshi, T.; Hatakeyama, S.; Shimono, A.; Sun, J. Y.; Zhang, Y. M.; Dzepina, K.; Kimmel, J. R.; Sueper, D.; Jayne, J. T.; Herndon, S. C.; Trimborn, A. M.; Williams, L. R.; Wood, E. C.; Middlebrook, A. M.; Kolb, C. E.; Baltensperger, U.; Worsnop, D. R. Evolution of organic aerosols in the atmosphere. *Science* **2009**, 326 (5959), 1525−9.

(3) Robinson, A. L.; Donahue, N. M.; Shrivastava, M. K.; Weitkamp, E. A.; Sage, A. M.; Grieshop, A. P.; Lane, T. E.; Pierce, J. R.; Pandis, S. N. Rethinking organic aerosols: Semivolatile emissions and photochemical aging. *Science* **2007**, 315**,** 1259–1262.

(4) Hallquist, M.; Wenger, J. C.; Baltensperger, U.; Rudich, Y.; Simpson, D.; Claeys, M.; Dommen, J.; Donahue, N. M.; George, C.; Goldstein, A. H.; Hamilton, J. F.; Herrmann, H.; Hoffmann, T.; Iinuma, Y.; Jang, M.; Jenkin, M. E.; Jimenez, J. L.; Kiendler-Scharr, A.; Maenhaut, W.; McFiggans, G.; Mentel, Th. F.; Monod, A.; Prévôt, A. S. H.; Seinfeld, J. H.; Surratt, J. D.; Szmigielski, R.; Wildt, J. The formation, properties and impact of secondary organic aerosol: current and emerging issues. *Atmos. Chem. Phys.* **2009**, 9, 5155–5236.

(5) Fu, T.-M.; Cao, J. J.; Zhang, X. Y.; Lee, S. C.; Zhang, Q.; Han, Y. M.; Qu,W. J.; Han, Z.; Zhang, R.; Wang, Y. X.; Chen, D.; Henze, D. K. Carbonaceous aerosols in China: top-down constraints on primary sources and estimation of secondary contribution. *Atmos. Chem. Phys.* **2012**, 12, 2725–2746.

(6) Jiang, F.; Liu, Q.; Huang, X.; Wang, T.; Zhuang, B.; Xie, M. Regional modeling of secondary organic aerosol over China using WRF/Chem. *J. Aerosol. Sci.* **2012**, 43, 57–73.

(7) Li, N.; Fu, T.-M.; Cao, J.; Lee, S.; Huang, X.-F.; He, L.-Y.; Ho, K.-F.; Fu, J. S.; Lam, Y.-F. Sources of secondary organic aerosols in the Pearl River Delta region in fall: Contributions from the aqueous reactive uptake of dicarbonyls. *Atmos. Environ.* **2013**, 76, 200–207.

(8) Tsai, I. C.; Chen, J.-P.; Lung, C. S.-C.; Li, N.; Chen, W.-N.; Fu, T.-M.; Chang, C.-C.; Hwang, G.-D. Sources and formation pathways of organic aerosol in a subtropical metropolis during summer. *Atmos. Environ.* **2015**, 117, 51–60.

(9) Feng, T.; Li, G.; Cao, J.; Bei, N.; Shen, Z.; Zhou, W.; Liu, S.; Zhang, T.; Wang, Y.; Huang, R.-J.; Tie, X.; Molina, L. T. Simulations of organic aerosol concentrations during springtime in the Guanzhong Basin, China. *Atmos. Chem. Phys.* **2016**, 16, 10045–10061.

(10) Han, Z.; Xie, Z.; Wang, G.; Zhang, R.; Tao, J. Modeling organic aerosols over east China using a volatility basis-set approach with aging mechanism in a regional air quality model. *Atmos. Environ.* **2016**, 124, 186–198.

(11) Chen, Q.; Fu, T.-M.; Hu, J. L.; Ying, Q.; Zhang, L. Modelling secondary organic aerosols in China. *Natl. Sci. Rev.* **2017,** 4, 806–809.

(12) Hu, J.; Wang, P.; Ying, Q.; Zhang, H.; Chen, J.; Ge, X.; Li, X.; Jiang, J.; Wang, S.; Zhang, J.; Zhao, Y.; Zhang, Y. Modeling biogenic and anthropogenic secondary organic aerosol in China. *Atmos. Chem. Phys.* **2017**, 17, 77–92.

(13) Xing, L.; Wu, J. R.; Elser, M.; Tong, S. R.; Liu, S. X.; Li, X.; Liu, L.; Cao, J.; Zhou, J. M.; El-Haddad, I.; Huang, R. J.; Ge, M. F.; Tie, X. X.; Prévôt, A. S. H.; Li, G. H. Wintertime secondary organic aerosol formation in Beijing–Tianjin–Hebei (BTH): contributions of HONO sources and heterogeneous reactions. *Atmos. Chem. Phys.* **2019**, 19**,** 2343-2359.

(14) Zheng, B.; Tong, D.; Li, M.; Liu, F.; Hong, C. P.; Geng, G. N.; Li, H. Y.; Li, X.; Peng, L. Q.; Qi, J.; Yan, L.; Zhang, Y. X.; Zhao, H. Y.; Zheng, Y. X.; He, K. B.; Zhang, Q. Trends in China's anthropogenic emissions since 2010 as the consequence of clean air actions. *Atmos. Chem. Phys.*

2018, 18**,** 14095-14111.

(15) Allan, J. D.; Williams, P. I.; Morgan, W. T.; Martin, C. L.; Flynn, M. J.; Lee, J.; Nemitz, E.; Phillips, G. J.; Gallagher, M. W.; Coe, H. Contributions from transport, solid fuel burning and cooking to primary organic aerosols in two UK cities. *Atmos. Chem. Phys.* **2010**, 10, 647–668.

(16) Huang, X. F.; He, L. Y.; Hu, M.; Canagaratna, M. R.; Sun, Y.; Zhang, Q.; Zhu, T.; Xue, L.; Zeng, L. W.; Liu, X. G.; Zhang, Y. H.; Jayne, J. T.; Ng, N. L.; Worsnop, D. R. Highly time-resolved chemical characterization of atmospheric submicron particles during 2008 Beijing Olympic Games using an Aerodyne High-Resolution Aerosol Mass Spectrometer. *Atmos. Chem. Phys.* **2010**, 10, 8933–8945.

(17) Mohr, C.; DeCarlo, P. F.; Heringa, M. F.; Chirico, R.; Slowik, J. G.; Richter, R.; Reche, C.; Alastuey, A.; Querol, X.; Seco, R.; Peñuelas, J.; Jiménez, J. L.; Crippa, M.; Zimmermann, R.; Baltensperger, U.; Prévôt, A. S. H. Identification and quantification of organic aerosol from cooking and other sources in Barcelona using aerosol mass spectrometer data. *Atmos. Chem. Phys.* **2012**, 12, 1649–1665.

(18) Crippa, M.; DeCarlo, P. F.; Slowik, J. G.; Mohr, C.; Heringa, M. F.; Chirico, R.; Poulain, L.; Freutel, F.; Sciare, J.; Cozic, J.; DiMarco, C. F.; Elsasser, M.; Nicolas, J. B.; Marchand, N.; Abidi, E.; Wiedensohler, A.; Drewnick, F.; Schneider, J.; Borrmann, S.; Nemitz, E.; Zimmermann, R.; Jaffrezo, J.-L.; Prévôt, A. S. H.; Baltensperger, U. Wintertime aerosol chemical composition and source apportionment of the organic fraction in the metropolitan area of Paris. *Atmos. Chem. Phys.* **2013**, 13, 961–981.

(19) Xu, L.; Suresh, S.; Guo, H.; Weber, R. J.; Ng, N. L. Aerosol characterization over the southeastern United States using high-resolution aerosol mass spectrometry: spatial and seasonal variation of aerosol composition and sources with a focus on organic nitrates. *Atmos. Chem. Phys.* **2015**, 15, 7307-7336.

(20) Xu, L.; Williams, L. R.; Young, D. E.; Allan, J. D.; Coe, H.; Massoli, P.; Fortner, E.; Chhabra, P.; Herndon, S.; Brooks, W. A.; Jayne, J. T.; Worsnop, D. R.; Aiken, A. C.; Liu, S.; Gorkowski, K.; Dubey, M. K.; Fleming, Z. L.; Visser, S.; Prévôt, A. S. H.; Ng, N. L. Wintertime aerosol chemical composition, volatility, and spatial variability in the greater London area. *Atmos. Chem. Phys.* **2016,** 16, 1139-1160.

(21) Elser, M.; Huang, R.-J.; Wolf, R.; Slowik, J. G.; Wang, Q.; Canonaco, F.; Li, G.; Bozzetti, C.;

Daellenbach, K. R.; Huang, Y.; Zhang, R.; Li, Z.; Cao, J.; Baltensperger, U.; El-Haddad, I.; Prévôt, A. S. H. New insights into $PM_{2.5}$ chemical composition and sources in two major cities in China during extreme haze events using aerosol mass spectrometry. *Atmos. Chem. Phys.* **2016**, 16, 3207–3225.

(22) Ots, R.; Vieno, M.; Allan, J. D.; Reis, S.; Nemitz, E.; Young, D. E.; Coe, H.; Marco, C. D.; Detournay, A.; Mackenzie, I. A.; Green, D. C.; Heal, M. R. Model simulations of cooking organic aerosol (COA) over the UK using estimates of emissions based on measurements at two sites in London. *Atmos. Chem. Phys.* **2016,** 16, 13773-13789.

(23) Cao, L. M.; Huang, X. F.; Li, Y. Y.; Hu, M.; He, L. Y. Volatility measurement of atmospheric submicron aerosols in an urban atmosphere in southern China. *Atmos. Chem. Phys.* **2018,** 18, 1729–1743.

(24) Sun, Y. L.; Zhang, Q.; Schwab, J. J.; Demerjian, K. L.; Chen, W. N.; Bae, M. S.; Hung, H. M.; Hogrefe, O.; Frank, B.; Rattigan, O. V.; Lin, Y. C. Characterization of the sources and processes of organic and inorganic aerosols in New York city with a high-resolution time-of-flight aerosol mass apectrometer. *Atmos. Chem. Phys.* **2011,** 11, 1581-1602.

(25) Sun, Y. L.; Xu, W. Q.; Zhang, Q.; Jiang, Q.; Canonaco, F.; Prévôt, A. S. H.; Fu, P. Q.; Li, J.; Jayne, J.; Worsnop, D. R.; Wang, Z. F. Source apportionment of organic aerosol from 2-year highly time-resolved measurements by an aerosol chemical speciation monitor in Beijing, China. *Atmos. Chem. Phys.* **2018,** 18, 8469-8489.

(26) Duan, J.; Huang, R. J.; Lin, C. S.; Dai, W. T.; Wang, M.; Gu, Y. F.; Wang, Y.; Zhong, H. B.; Zheng, Y.; Ni, H. Y.; Dusek, U.; Chen, Y.; Li, Y. J.; Chen, Q.; Worsnop, D. R.; O'Dowd, C.; Cao, J. J. Distinctions in source regions and formation mechanisms of secondary aerosol in Beijing from summer to winter. *Atmos. Chem. Phys.* **2019,** 19, 10319–10334.

(27) Liu, T. Y.; Zhou, L. Y.; Liu, Q. Y.; Lee, B. P.; Yao, D. W.; Lu, H. X.; Lyu, X. P.; Guo, H.; Chan, C. K. Secondary Organic Aerosol Formation from Urban Roadside Air in Hong Kong. *Environ. Sci. Technol.* **2019,** 53, 3001−3009.

(28) Lee, B. P.; Li, Y. J.; Yu, J. Z.; Louie, P. K. K.; Chan, C. K. Characteristics of submicron particulate matter at the urban roadside in downtown Hong Kong—Overview of 4 months of continuous high-resolution aerosol mass spectrometer measurements. *J. Geophys. Res.-Atmos.* **2015,** 120, 7040 – 7058.

(29) Sun, C.; Lee, B. P.; Huang, D.; Li, Y. J.; Schurman, M. I.; Louie, P. K. K.; Chan, C. K. Continuous measurements at the urban roadside in an Asian megacity by Aerosol Chemical Speciation Monitor (ACSM): particulate matter characteristics during fall and winter seasons in Hong Kong. *Atmos. Chem. Phys.* **2016,** 16, 1713–1728.

(30) Qin, Y. M.; Tan, H. B.; Li, Y. J.; Schurman, M. I.; Li, F.; Canonaco, F.; Prévôt, A. S. H.; Chak, C. K. Impacts of traffic emissions on atmospheric particulate nitrate and organics at a downwind site on the periphery of Guangzhou, China. *Atmos. Chem. Phys.* **2017,** 17, 10245–10258.

(31) Wang, L. N.; Xiang, Z. Y.; Stevanovic, S.; Ristovski, Z.; Salimi, F.; Gao, J.; Wang, H. L.; Li, L. Role of Chinese cooking emissions on ambient air quality and human health. *Sci. Total Environ.* **2017,** 589, 173–181.

(32) He, L. Y.; Hu, M.; Huang, X. F.; Yu, B. D.; Zhang, Y. H.; Liu, D. Q. Measurement of emissions of fine particulate organic matter from Chinese cooking. *Atmos. Environ.* **2004,** 38, 6557–6564.

(33) Fountoukis, C.; Megaritis, A. G.; Skyllakou, K.; Charalampidis, P. E.; Denier van der Gon, H. A. C.; Crippa, M.; Prévôt, A. S. H.; Fachinger, F.; Wiedensohler, A.; Pilinis, C.; Pandis, S. N. Simulating the formation of carbonaceous aerosol in a European Megacity (Paris) during the MEGAPOLI summer and winter campaigns. *Atmos. Chem. Phys.* **2016,** 16, 3727–3741.

(34) Zhai, S. X.; Jacob, D. J.; Wang, X.; Shen, L.; Li, K.; Zhang, Y. Z.; Gui, K.; Zhao, T. L.; Liao, H. Fine particulate matter ($PM_{2.5}$) trends in China, 2013–2018: separating contributions from anthropogenic emissions and meteorology. *Atmos. Chem. Phys.* **2019,** 19, 11031-11041.

(35) Ye, T. T.; Zhao, N. Z.; Yang, X. C.; Ouyang, Z. T.; Liu, X. P.; Chen, Q.; Hu, K. J.; Yue, W. Z.; Qi, J. G.; Li, Z. S.; Jia. P. Improved population mapping for China using remotely sensed and points-of-interest data within a random forests model. *Sci. Total Environ.* **2019,** 658, 936–946.

(36) Hua, J. Y.; Zhang, X. Y.; Ren, C.; Shi, Y.; Lee, T. C. Spatiotemporal assessment of extreme heat risk for high-density cities: A case study of Hong Kong from 2006 to 2016. *Sustain. Cities Soc.* **2021**, 64, 102507.

(37) Dobson, J. E.; Bright, E. A.; Coleman, P. R.; Durfee, R. C.; Worley, B. A. LandScan: A global population database for estimating populations at risk *Photogramm Eng Remote Sens.* **2000,** 66, 849–857.

(38) Li, G.; Lei, W.; Zavala, M.; Volkamer, R.; Dusanter, S.; Stevens, P.; Molina, L. T. Impacts of HONO sources on the photochemistry in Mexico city during the MCMA-2006/MILAGO

campaign. *Atmos. Chem. Phys.* **2010,** 10, 6551-6567.

(39) Li, G.; Bei, N.; Tie, X.; Molina, L. T. Aerosol effects on the photochemistry in Mexico City during MCMA-2006/MILAGRO campaign. *Atmos. Chem. Phys.* **2011a,** 11, 5169-5182

(40) Li, G.; Zavala, M.; Lei, W.; Tsimpidi, A. P.; Karydis, V. A.; Pandis, S. N.; Canagaratna, M. R.; Molina, L. T. Simulations of organic aerosol concentrations in Mexico City using the WRF-CHEM model during the MCMA-2006/MILAGRO campaign. *Atmos. Chem. Phys.* **2011b,** 11, 3789-3809.

(41) Li, G.; Lei, W.; Bei, N.; Molina, L. T. Contribution of garbage burning to chloride and $PM_{2.5}$ in Mexico City. *Atmos. Chem. Phys.* **2012,** 12, 8751-8761.

(42) Binkowski, F. S.; Roselle, S. J. Models-3 community multiscale air quality (CMAQ) model aerosol component –1. Model description. *J. Geophys. Res.-Atmos.* **2003,** 108, 4183.

(43) Shrivastava, M.; Lane, T. E.; Donahue, N. M.; Pandis, S. N.; Robinson, A. L. Effects of gas particle partitioning and aging of primary emissions on urban and regional organic aerosol concentrations. *J. Geophys. Res.-Atmos.* **2008,** 113, D18301.

(44) Liu, T. Y.; Wang, Z. Y.; Wang, X. M.; Chan, C. K. Primary and secondary organic aerosol from heated cooking oil emissions. *Atmos. Chem. Phys.* **2018,** 18, 11363–11374.

(45) Liu, T. Y.; Li, Z. J.; Chan, M. N.; Chan, C. K. Formation of secondary organic aerosols from gas-phase emissions of heated cooking oils. *Atmos. Chem. Phys.* **2017,** 17, 7333–7344.

(46) Liu, T. Y.; Wang, Z. Y.; Huang, D. D.; Wang, X. M.; Chan, C. K. Significant Production of Secondary Organic Aerosol from Emissions of Heated Cooking Oils. *Environ. Sci. Technol. Lett.* **2018,** 5, 32−37.

(47) Zhang, Z. R.; Zhu, W. F.; Hu, M.; Wang, H.; Chen, Z.; Shen, R. Z.; Yu, Y.; Tan, R.; Guo, S. Secondary Organic Aerosol from Typical Chinese Domestic Cooking Emissions. *Environ. Sci. Technol. Lett.* **2020,** 8, 24-31.

(48) Morrison, H.; Thompson, G.; Tatarskii, V. Impact of cloud microphysics on the development of trailing stratiform precipitation in a simulated squall line: comparison of one- and two-moment schemes. *Mon. Weather Rev.* **2009,** 137, 991-1007.

(49) Chou, M. D.; Suarez, M. J. A solar radiation parameterization for atmospheric studies. *NASA/TM-1999-104606 NASA Tech. Memo.* **1999,** 15, 40.

(50) Chou, M. D.; Suarez, M. J.; Liang, X. Z.; Yan, M. H.; Cote, C. A thermal infrared radiation

parameterization for atmospheric studies. *NASA/TM-2001-104606 Tech. Rep.* **2001,** 19, 55.

(51) Janjić, Z. I. Nonsingular Implementation of the Mellor-Yamada Level 2.5 Scheme in the NCEP Meso Model *Ncep Office Note* **2002,** 437, 61.

(52) Chen, F.; Dudhia, J. Coupling an advanced land surface-hydrology model with the Penn State-NCAR MM5 modeling system. Part I: Model implementation and sensitivity. *Mon. Weather Rev.* **2001,** 129, 569-585.

(53) Horowitz, L. W.; Walters, S.; Mauzerall, D. L.; Emmons, L. K.; Rasch, P. J.; Granier, C.; Tie, X. X.; Lamarque, J. F.; Schultz, M. G.; Tyndall, G. S.; Orlando, J. J.; Brasseur, G. P. A global simulation of tropospheric ozone and related tracers: Description and evaluation of MOZART, version 2. *J. Geophys. Res.-Atmos.* **2003,** 108, 4784.

(54) Zhang, Q.; Streets, D. G.; Carmichael, G. R.; He, K. B.; Huo, H.; Kannari, A.; Klimont, Z.; Park, I. S.; Reddy, S.; Fu, J. S.; Chen, D.; Duan, L.; Lei, Y.; Wang, L. T.; Yao, Z. L. Asian emissions in 2006 for the NASA INTEX-B mission. *Atmos. Chem. Phys.* **2009,** 9, 5131–5153.

(55) Wiedinmyer, C.; Quayle, B.; Geron, C.; Belote, A.; McKenzie, D.; Zhang, X.; O'Neill, S.; Wynne, K. K. Estimating emissions from fires in North America for air quality modeling. *Atmos. Environ.* **2006,** 40, 3419-3432.

(56) Wiedinmyer, C.; Akagi, S. K.; Yokelson, R. J.; Emmons, L. K.; Al-Saadi, J. A.; Orlando, J. J.; Soja, A. J. The Fire INventory from NCAR (FINN): a high resolution global model to estimate the emissions from open burning. *Geosci. Model Dev.* **2011,** 4, 625-641.

(57) Guenther, A.; Karl, T.; Harley, P.; Wiedinmyer, C.; Palmer, P. I.; Geron, C. Estimates of global terrestrial isoprene emissions using MEGAN (Model of Emissions of Gases and Aerosols from Nature). *Atmos. Chem. Phys.* **2006,** 6, 3181–3210.

(58) Guo, J. C.; Zhou, S. S.; Cai, M. F.; Zhao, J.; Song, W.; Zhao, W. X.; Hu, W. W.; Sun, Y. L.; He, Y.; Yang, C. Q.; Xu, X. Z.; Zhang, Z. S.; Cheng, P.; Fan, Q.; Hang, J.; Fan, S. J.; Wang, X. M.; Wang, X. M. Characterization of submicron particles by time-of-flight aerosol chemical speciation monitor (ToF-ACSM) during wintertime: aerosol composition, sources, and chemical processes in Guangzhou, China. *Atmos. Chem. Phys.* **2020,** 20, 7595–7615.

(59) Xing, L.; Fu, T. M.; Cao, J. J.; Lee, S. C.; Wang, G. H.; Ho, K. F.; Cheng, M. C.; You, C. F.; Wang, T. J. Seasonal and spatial variability of the OM/OC mass ratios and high regional correlation between oxalic acid and zinc in Chinese urban organic aerosols. *Atmos. Chem. Phys.* **2013,** 13,

4307-4318.

Figure Captions

Figure 1 WRF-Chem model domain with the population density. The black hollow circles denote the centers of cities that have ambient monitoring sites, and the sizes of the circles denote the number of ambient monitoring sites in the cities. The inset shows the population density in the PRD region. The two blue circles in the inset represents the location of the urban roadside site at the Hong Kong Polytechnic University (PolyU) (22.30 °N, 114.18 °E) and Panyu Atmospheric Composition station at Guangzhou (Panyu) (23.00 °N, 113.21 °E). The two black circles in the inset represent the locations of two urban sites in Shenzhen (22.60 °N, 113.90 °E) and Guangzhou (23.08 °N, 113.21 °E).

Figure 2 Comparisons of observed (black dots) and simulated (red lines) temporal variations of (a) $PM_{2.5}$ concentrations averaged at the ambient monitoring sites, (b) HOA concentrations, (c) COA concentrations, and (d) SOA concentrations at the PolyU site from December 27, 2017 to January 15, 2018.

Figure 3 The diurnal cycles of observed (black dots) and simulated (red and blue lines) COA concentrations on weekdays ((a) PolyU site and (c) Panyu site) and weekends ((b) PolyU site and (d) Panyu site).

Figure 4 The diurnal variations of COA emission percentages on weekdays (red lines) and weekends (blue lines) in the PRD region in winter.

Figure 5 The spatial distributions of (a) COA emissions, (b) COA concentrations, and (c) COA mass fractions to OA over the PRD region averaged from December 27, 2017 to January 15, 2018.

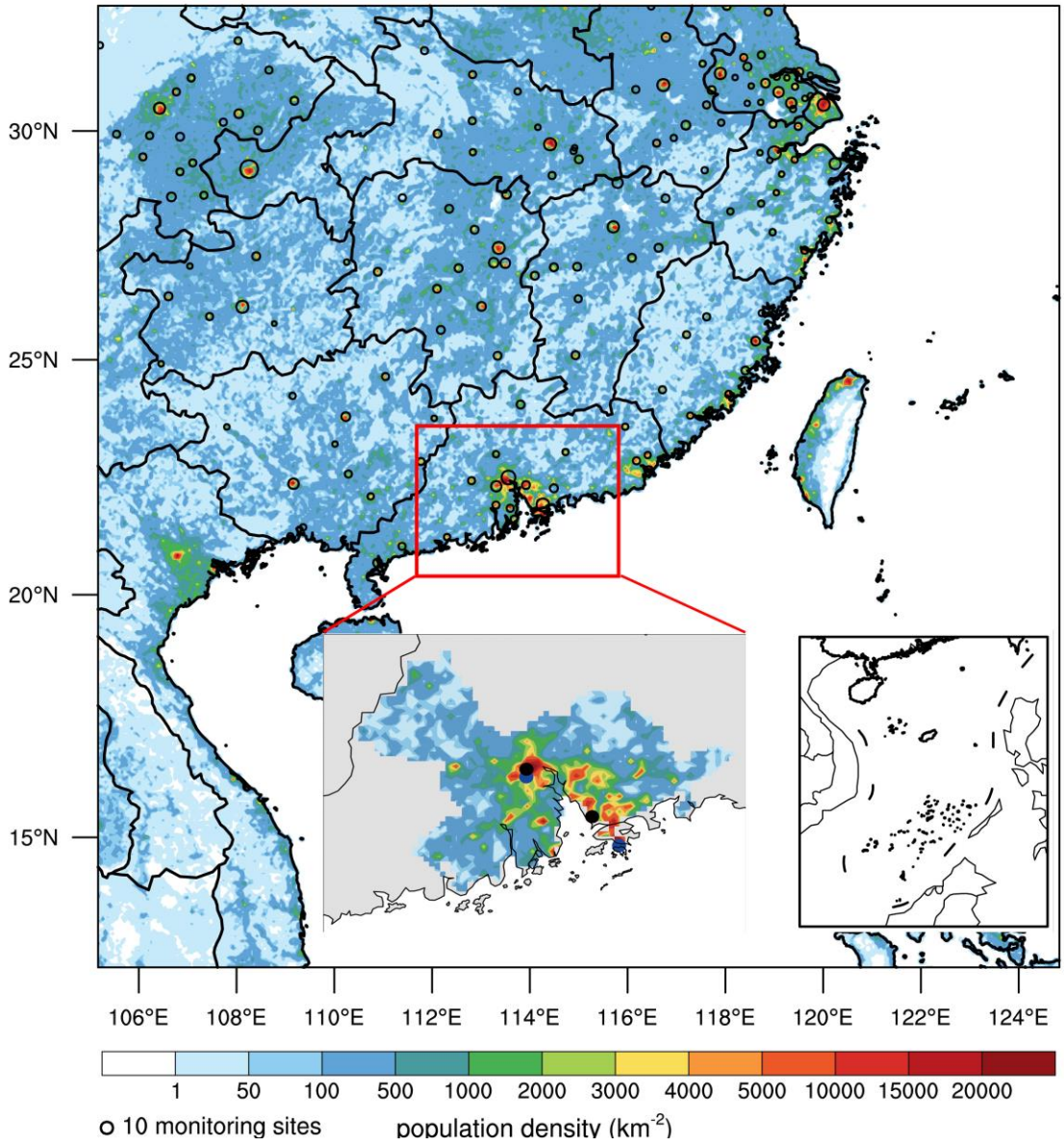

Figure 1 WRF-Chem model domain with the population density. The black hollow circles denote the centers of cities that have ambient monitoring sites, and the sizes of the circles denote the number of ambient monitoring sites in the cities. The inset shows the population density in the PRD region. The two blue circles in the inset represents the location of the urban roadside site at the Hong Kong Polytechnic University (PolyU) (22.30 °N, 114.18 °E) and Panyu Atmospheric Composition station at Guangzhou (Panyu) (23.00 °N, 113.21 °E). The two black circles in the inset represent the locations of two urban sites in Shenzhen (22.6 °N, 113.9 °E) and Guangzhou (23.08 °N, 113.21 °E).

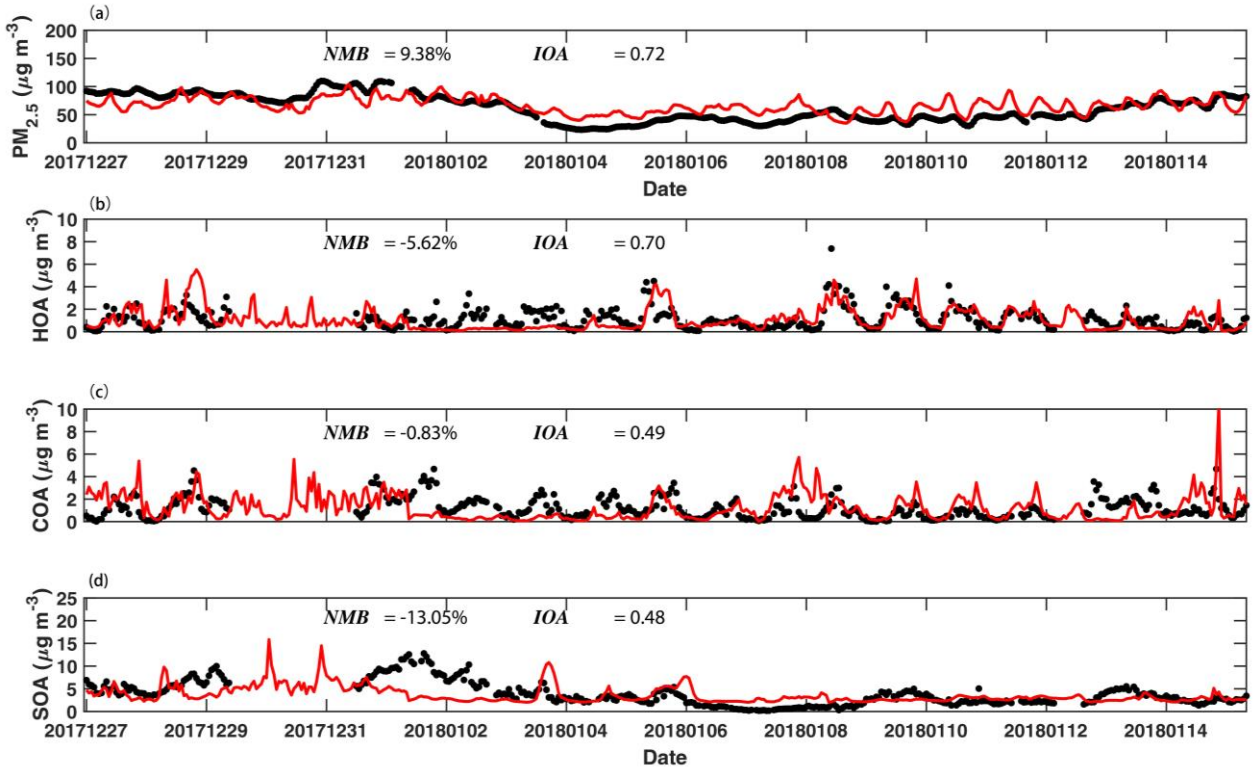

Figure 2 Comparisons of observed (black dots) and simulated (red lines) temporal variations of (a) $PM_{2.5}$ concentrations averaged at the ambient monitoring sites, (b) HOA concentrations, (c) COA concentrations, and (d) SOA concentrations at the PolyU site from December 27, 2017 to January 15, 2018.

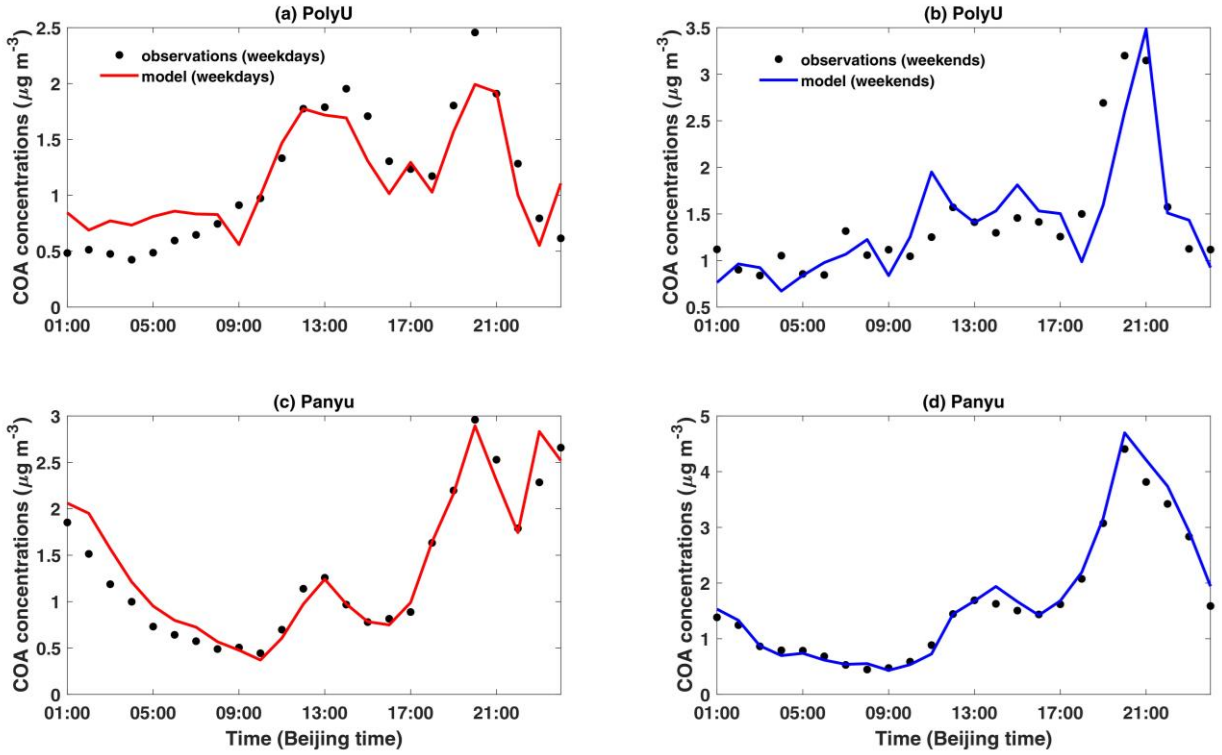

Figure 3 The diurnal cycles of observed (black dots) and simulated (red and blue lines) COA concentrations on weekdays ((a) PolyU site and (c) Panyu site) and weekends ((b) PolyU site and (d) Panyu site).

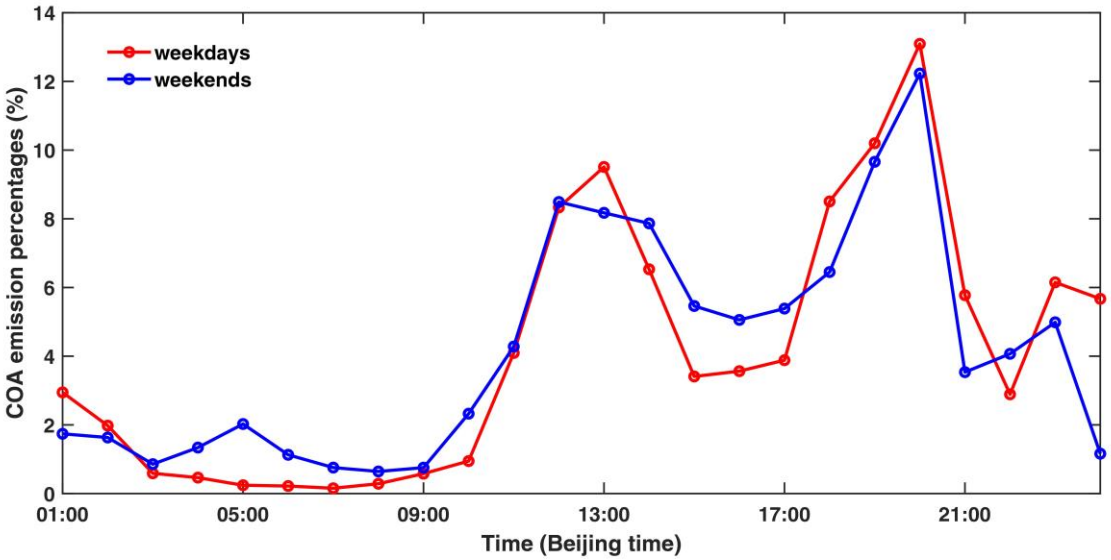

Figure 4 The diurnal variations of COA emission percentages on weekdays (red lines) and weekends (blue lines) in the PRD region in winter.

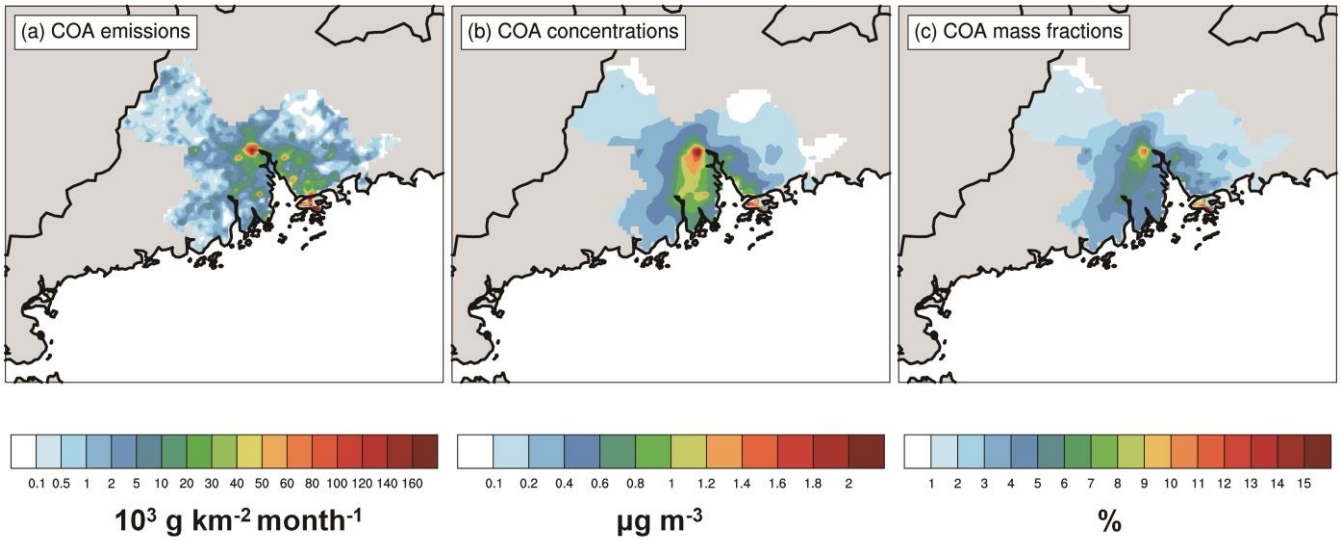

Figure 5 The spatial distributions of (a) COA emissions, (b) COA concentrations, and (c) COA mass fractions to OA over the PRD region averaged from December 27, 2017 to January 15, 2018.